## Phase Separation Induced by Orbital Degrees of Freedom in Models for Manganites with Jahn-Teller Phonons

S. Yunoki, A. Moreo, and E. Dagotto
National High Magnetic Field Lab and Department of Physics, Florida State University, Tallahassee, FL 32306
(December 2, 2024)

The two-orbital Kondo model with classical Jahn-Teller phonons is studied using Monte Carlo techniques. The observed phase diagram is rich, and includes a novel regime of phase separation induced by the orbital degrees of freedom. Experimental consequences of our results are discussed. In addition, the optical conductivity  $\sigma(\omega)$  of the model is presented. It is shown to have several similarities with experimental measurements for manganites.

PACS numbers: 71.10.-w, 75.10.-b, 75.30.Kz

The properties of doped manganites are currently under much investigation due to the dramatic decrease in their resistivity when the spins order ferromagnetically by lowering the temperature T or applying a magnetic field [1]. This effect is caused by a metal-insulator transition associated with the magnetic ordering. The existence of the ferromagnetic (FM) phase is understood based on the double-exchange (DE) mechanism [2]. However, experiments on manganites have revealed a complicated phase diagram that also includes charge-ordered and antiferromagnetic (AF) phases [3]. This rich structure is beyond the DE ideas and a more refined approach is needed to understand these compounds.

Since the 1950s the 1-orbital FM Kondo model for manganites has been widely studied. However, it is only recently that its computational analysis started, and surprises have already been observed [4–6]. In particular, the transition from the undoped spin-AF regime to the spin-FM regime at finite hole-density occurs through phase separation (PS), instead of through a canted state as believed before. A growing body of experimental results indeed indicate the existence of PS in manganites [7,8], in agreement with the theoretical calculations. It is conceivable that PS tendencies above the FM critical temperature  $T_c^{FM}$  could be important to explain the colossal magnetoresistance of doped manganites.

However, in spite of its rich phase diagram the 1-orbital Kondo model is incomplete for a full description of Mnoxides. For instance, dynamical Jahn-Teller (JT) distortions are also important [9], and a proper description of the recently observed orbital order [10] obviously needs at least two orbitals. Such a multi-orbital model with JT phonons is nontrivial [11], and the previous experience with the 1-orbital case suggests that a computational analysis is crucial to understand its properties. In addition, it is conceptually interesting to analyze whether PS [4,5] exists also in multi-orbital models.

It is precisely the purpose of this paper to report the first computational study of a 2-orbital model for manganites including JT phonons. The results show a rich

phase diagram including a novel regime of PS induced by the orbital, rather than the spin, degrees of freedom (DOF). The Hamiltonian used here has three contributions  $H_{KJT} = H_K + H_{JT} + H_{AF}$ . The first term is

$$H_K = -\sum_{\langle \mathbf{i}\mathbf{j}\rangle\sigma ab} t_{ab} (c_{\mathbf{i}a\sigma}^{\dagger} c_{\mathbf{j}b\sigma} + h.c.) - J_H \sum_{\mathbf{i}a\alpha\beta} \mathbf{S_i} \cdot c_{\mathbf{i}a\alpha}^{\dagger} \sigma_{\alpha\beta} c_{\mathbf{i}a\beta},$$

where  $\langle \mathbf{ij} \rangle$  denotes nearest-neighbor lattice sites,  $J_H > 0$  is the Hund coupling, a, b = 1, 2 are the two  $e_g$ -orbitals, the  $t_{2g}$ -spins  $\mathbf{S_i}$  are assumed to be classical (with  $|\mathbf{S_i}| = 1$ ) since their actual value in Mn-oxides (3/2) is large [12], and the rest of the notation is standard. None of the results described below depends crucially on the set  $\{t_{ab}\}$  selected [13]. Throughout the paper the energy units are chosen such that  $t_{11} = 1$  in the x-direction. In addition, since  $J_H$  is large in the real manganites, here it will be fixed to 8 unless otherwise stated. Finally, the  $e_g$ -density  $\langle n \rangle$  is adjusted using a chemical potential  $\mu$ .

The coupling with JT-phonons is through [9]

$$H_{JT} = \lambda \sum_{\mathbf{i}ab\sigma} c_{\mathbf{i}a\sigma}^{\dagger} Q_{\mathbf{i}}^{ab} c_{\mathbf{i}b\sigma} + \frac{1}{2} \sum_{\mathbf{i}} (Q^{(2)}_{\mathbf{i}}^{2} + Q^{(3)}_{\mathbf{i}}^{2}), \quad (2)$$

where  $Q_{\mathbf{i}}^{11}=-Q_{\mathbf{i}}^{22}=Q_{\mathbf{i}}^{(3)}$ , and  $Q_{\mathbf{i}}^{12}=Q_{\mathbf{i}}^{21}=Q_{\mathbf{i}}^{(2)}$ . These phonons are assumed to be classical. This approximation has been used and discussed in previous literature [9], where it was concluded that at temperatures of the order of the critical ones (room temperature), or a sizable fraction of them, the use of classical phonons captures the important physics of the model [14]. Certainly at very low-temperatures the quantum character of phonons is important, but this is not the range of temperatures explored in the present paper. Note that here T = 1/10 is about 200-300K [4]. Finally, a small coupling between the  $t_{2q}$ -spins is needed to account for the AF character of the real materials even when all La is replaced by Ca. This classical Heisenberg term is  $H_{AF} = J' \sum_{\langle ij \rangle} \mathbf{S}_i \cdot \mathbf{S}_j$ , where J' is fixed to 0.05 throughout the paper, a value compatible with experiments [15]. To study  $H_{KJT}$  a Monte Carlo (MC)

technique was used. The trace over the  $e_g$ -electrons is carried out exactly using library subroutines for a fixed background of  $t_{2g}$ -spins and phonons. This background is selected based on a Metropolis MC procedure [4]. The CPU time of the technique grows rapidly with the number of sites L, but the method has the important advantage that it does not have sign-problems at any T [4]. Finally, to analyze orbital correlations the pseudopin operator  $\mathbf{T_i} = \frac{1}{2} \sum_{\sigma ab} c^{\dagger}_{\mathbf{i}a\sigma} \sigma_{ab} c_{\mathbf{i}b\sigma}$  is used, while for spin correlations the operator is standard. The Fourier-transform of the pseudospin correlations is defined as  $T(\mathbf{q}) = \frac{1}{L} \sum_{\mathbf{l},\mathbf{m}} e^{i\mathbf{q}\cdot(\mathbf{l}-\mathbf{m})} \langle \mathbf{T_m} \cdot \mathbf{T_l} \rangle$ , with a similar definition for the spin structure factor  $S(\mathbf{q})$ .

Consider first the limit  $\langle n \rangle = 1.0$  (undoped manganites). Fig.1a shows T(q) and S(q) at representative momenta vs.  $\lambda$ . For small  $\lambda$  a large S(0) indicates a tendency to spin-FM order induced by DE (as in the qualitatively similar 1-orbital problem at  $\langle n \rangle = 0.5$  [4]). The small values of T(q) imply that in this regime the orbitals remain disordered. When the coupling reaches  $\lambda_{c1} \sim 1.0$ , the rapid increase of  $T(\pi)$  now suggests that the ground state has a tendency to form a *staggered* (or "antiferro") orbital pattern, with the spins remaining FM aligned since S(0) is large [16]. The existence of this phase was discussed before, but using multi-orbital Hubbard models without phonons [17]. Our results show that it can be induced by JT phonons. As the coupling increases further, another transition at  $\lambda_{c2} \sim 2.0$  occurs to a spin-AF orbital-FM state  $(S(\pi))$  and T(0) are large). In this region a 1-orbital approximation is suitable. Studying the spin and orbital correlations in real-space leads to the same conclusions as discussed here.

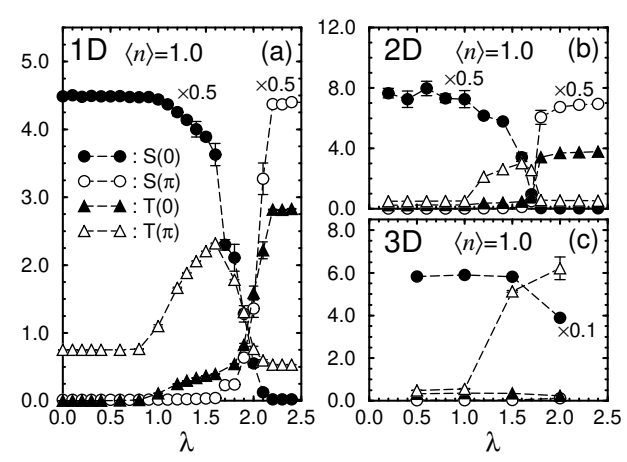


FIG. 1. (a) T(q) and S(q) vs  $\lambda$ , working at  $\langle n \rangle = 1.0$ , T = 1/75,  $J_H = 8$ , J' = 0.05, and in 1D with 10 sites.  $\{t_{ab}\}$  correspond to set  $T_1$  (see [13]); (b) Same as (a) but for a  $4^2$  cluster, T = 1/50, and hopping  $T_3$  ( $T_4$ ) in the y (x) direction.  $q = 0(\pi)$  denotes (0,0) ( $(\pi,\pi)$ ); (c) Same as (a) but for a  $4^3$  cluster, T = 1/50, the 3D hopping amplitudes of Ref. [13], and  $J_H = \infty$ .  $q = 0(\pi)$  denotes (0,0,0) ( $(\pi,\pi,\pi)$ ).

The three regimes of Fig.1a can be understood in the

limit where  $\lambda$  and  $J_H$  are the largest scales, and using  $t_{12}=t_{21}=0,\ t_{11}=t_{22}=t$  for simplicity. For parallel spins with orbitals split in a staggered (uniform) pattern, the energy per site at lowest order in t is  $\sim -t^2/\Delta$  ( $\sim$  0), where  $\Delta$  is the orbital splitting. For antiparallel spins with uniform (staggered) orbital splitting, the energy is  $\sim -t^2/2J_H\ (\sim -t^2/(2J_H+\Delta))$ . Then, when  $\Delta < 2J_H\ ($ "intermediate"  $\lambda$ s), a spin-FM orbital-AF order dominates, while as  $\lambda$  grows further a transition to a spin-AF orbital-FM ground state is expected. This reasoning is dimension independent, as the results for a 2D cluster in Fig.1b show. In 3D (Fig.1c) and  $J_H=\infty$  at least two of the regimes of Fig.1a-b have been identified [18]. It was also observed that the behavior in Fig.1a-b does not change when other sets  $\{t_{ab}\}$  are used [13].

The next issue to be explored are the transport properties in the three regimes at  $\langle n \rangle = 1$ . The algorithm used here allows us to calculate real-time dynamical responses accurately, including the optical conductivity  $\sigma(\omega > 0)$ , since all the eigenvectors in the fermionic sector for a given spin and phonon configuration are obtained exactly [5]. From the sum-rule,  $e_g$  kinetic-energy, and the integral of  $\sigma(\omega>0)$ , the  $\omega=0$  Drude-weight  $D_W$  can be obtained. In Fig.2a,  $D_W$  is shown for several sizes.  $D_W$  vanishes at  $\lambda_{c1}$  signaling a metal-insulator transition (MIT). Here the insulating phase is spin-FM and orbital-AF, while the metallic one is spin-FM and orbitaldisordered [19]. The density of states (DOS) for  $\lambda > \lambda_{c1}$ was also calculated and it presents a clear gap at the Fermi level. Although finite-size studies for D > 1 are difficult, the qualitative shape of  $D_W$  vs  $\lambda$  on  $4^2$  and  $4^3$ clusters was found to be the same as in 1D and, thus, it is likely that the MIT exists also in D=2 and 3.

Consider now the influence of hole doping on the  $\langle n \rangle = 1.0$  phase diagram. The first issue to be addressed is the stability of other densities as  $\mu$  is varied. Fig.2b shows  $\langle n \rangle$  vs  $\mu$  in the intermediate- $\lambda$  regime. It is remarkable that two regions of unstable densities exist below some critical temperature  $T_c^{PS}$  (roughly  $\sim 1/20$ , see inset Fig.2b). Similar conclusions were reached using the Maxwell's construction [5]. Over 10<sup>6</sup> MC sweeps at each  $\mu$  were needed for convergence near the unstable regions. These instabilities signal the existence of PS in the  $H_{KJT}$ model. At low-density there is separation between an (i) empty  $e_q$ -electron band with AF-ordered  $t_{2q}$ -spins and a (ii) metallic spin-FM orbital-FM phase. In the unstable region near  $\langle n \rangle = 1.0 \text{ PS}$  is between the phase (ii) mentioned above, and (iii) the insulating spin-FM and orbital-AF phase described in Fig.1a [20]. The driving force for this novel regime of PS are the orbital DOF, since the spins are uniformly ordered in both phases involved. Studying  $\langle n \rangle$  vs  $\mu$ , for  $\lambda < \lambda_{c1}$  only PS at small densities is observed, while for  $\lambda > \lambda_{c2}$  the PS close to  $\langle n \rangle = 1$  involves a spin-AF orbital-FM phase [4].

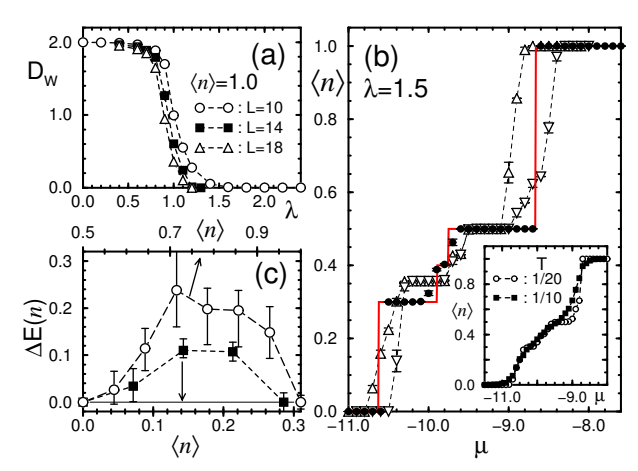


FIG. 2. (a)  $D_W$  vs  $\lambda$  for several chains (T=1/75); (b)  $\langle n \rangle$  vs  $\mu$  at  $\lambda=1.5$ , L=10, and T=1/40 (solid circles). The solid line is obtained from the Maxwell's construction. The triangles are results also at  $\lambda=1.5$  and T=1/40, but using 14 sites and only  $2\times 10^4$  MC sweeps to show the appearance of hysteresis loops as in a first-order transition. The inset shows the T-dependence of the results at L=10; (c)  $\Delta E(n)$  (see text) vs  $\langle n \rangle$  showing a negative curvature characteristic of PS. Results at large (open circles) and small (full squares) densities are shown, on a L=14 cluster with periodic boundary conditions and the couplings of (b).

To confirm that the discontinuity in  $\langle n \rangle$  vs  $\mu$  corresponds to phase separation, in Fig.2c the ground state energy is provided at several densities. The results indeed have the negative curvature characteristic of PS, both at large and small densities. To accommodate the two important density regimes in the same plot, the energies in Fig.2c are defined as  $\Delta E(n) = E(n) - E_0(n)$ , where E(n) is the actual ground state energy obtained as explained in Ref. [5], and  $E_0(n)$  is a straight line (zero curvature) that joins the energies of the two (stable) extremal densities of both the low- and high-density regimes. Further confirmation of the PS tendencies was obtained by inspecting the MC time-evolution of the density, as  $\mu$  is varied. While at the critical  $\mu$  frequent tunneling events were observed, at other  $\mu$ 's the time-evolution was smooth.

Results in the limit  $J_H = \infty$  using a L = 22 site cluster have also been obtained (see Fig.3a). Once again, a discontinuity in  $\langle n \rangle$  vs  $\mu$  was found at large and small densities, correlated with a negative curvature in the energy (not shown). Fig.3a helps in clarifying that the plateaus at densities, e.g., between 0.3 and 0.5 in Fig.2c are caused by the intrinsic discreteness of the clusters used here. As L grows, this fine structure disappears. See, e.g., the smoothly varying density between  $\langle n \rangle \sim 0.25$  and  $\sim 0.55$  in Fig.3a. However, the discontinuities at large and small  $\langle n \rangle$  remain strong, as they should if there is PS in the problem. Note that similar results as found in 1D appear also in studies of 2D systems (Fig.3b).

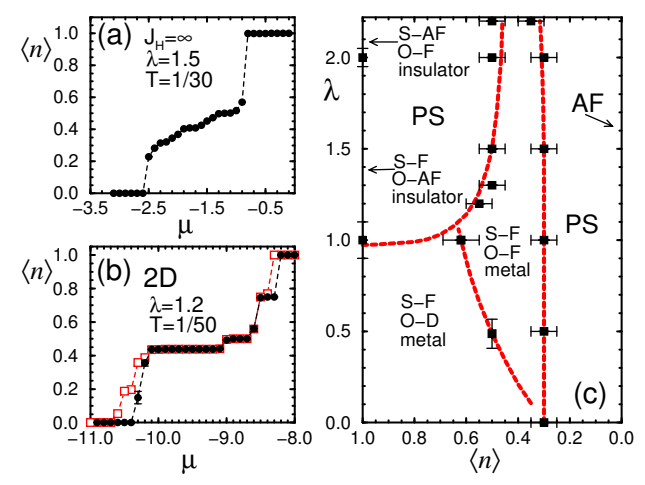


FIG. 3. (a)  $\langle n \rangle$  vs  $\mu$  in the limit  $J_H = \infty$ , using  $\lambda = 1.5$ , J' = 0.05, T = 1/30, and a 22-site chain; (b)  $\langle n \rangle$  vs  $\mu$  at  $\lambda = 1.2$  using a  $4^2$  cluster and at T = 1/50. The two sets of points that produce the hysteresis loops are obtained by increasing and decreasing  $\mu$  using  $\sim 10^4$  sweeps at each  $\mu$ ; (c) Phase diagram of  $H_{KJT}$  at  $J_H = 8.0$ , J' = 0.05, and using set  $T_1$  for  $\{t_{ab}\}$ . S – F and S – AF denote regimes with FM- and AF-spin order, respectively. O – D, O – F, and O – AF represent states with disordered, uniform and staggered orbital order, respectively. PS means phase separation.

Then, based on the information discussed thus far, supplemented by other MC measurements, the phase diagram of the 1D  $H_{KJT}$  model is given in Fig.3c. The metallic spin-FM region contains two regimes: one ferrorbital ordered and the other orbitally disordered, as deduced from the behavior of pseudospin correlations, the mean-value of the pseudospin operators, and the probability of double occupancy of the same site with different orbitals. The results are similar for several  $\{t_{ab}\}$  sets [13]. Our simulations suggest that the qualitative shape of Fig.3c should be valid also in D=2 and 3.

Consider now  $\sigma(\omega)$ . Experimental studies for a variety of manganites reported a broad peak at  $\omega \sim 1eV$  (for hole doping x>0.2 and  $T>T_c^{FM}$ ) [21,22]. At room-T there is negligible weight near  $\omega=0$ , but as T is reduced the 1eV-peak shifts to smaller energies, gradually transforming into a Drude response well below  $T_c^{FM}$ . The finite- $\omega$  peak can be identified even inside the FM phase. The coherent spectral weight is only a small fraction of the total. Other features at larger energies  $\sim 3eV$  involve transitions between the  $J_H$ -split bands and the O-ions.

In Fig.4a,  $\sigma(\omega)$  for the  $H_{KJT}$  model is shown at  $\langle n \rangle = 0.7$  and several temperatures near the unstable PS region of Fig.3c (weight due to  $J_H$  split bands is not shown, but it appears at higher energy). Here the FM spin correlation length grows rapidly with the lattice size for  $T^* \leq 0.05t$ , which can be considered as the "critical" temperature. Both at high- and intermediate-T a broad peak is observed at  $\omega \sim 1$ , smoothly evolving to lower energies as T decreases. The peak can be identified below

 $T^*$  as in experiments [21,22]. Eventually as the temperature is further reduced,  $\sigma(\omega)$  is dominated by a Drude peak. The T-dependence shown in Fig.4a is achieved at this  $\lambda$  and  $\langle n \rangle$  by a combination of a finite- $\omega$  phonon-induced broad feature that loses weight, and a Drude response that grows as T decreases (for smaller  $\lambda$ s, the two peaks can be distinguished even at the lowest temperature shown in Fig.4a). The similarity with experiments suggests that real manganites may have couplings close to an unstable region in parameter space. In the inset,  $D_W$  vs T is shown. Note that  $D_W$  vanishes suggesting a MIT, probably due to polaron localization. Results for the 1-orbital case are smoother.

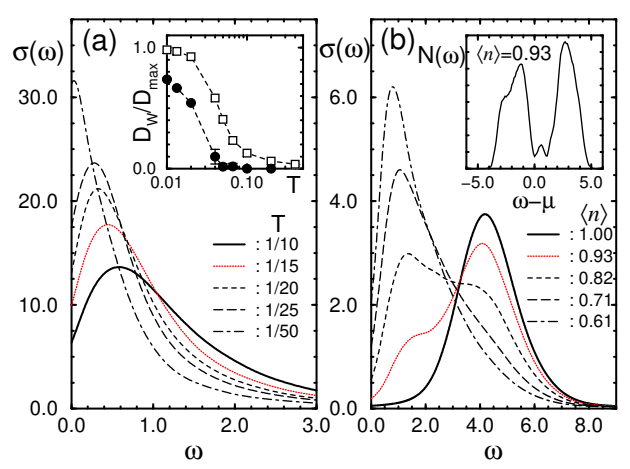


FIG. 4. (a)  $\sigma(\omega)$  at  $\lambda=1.0$ ,  $\langle n\rangle=0.7$ , and L=20, and several temperatures. The inset shows  $D_W$  vs T for both the  $H_{KJT}$  (circles) and the 1-orbital model (squares) of Ref. [4] (the latter at  $\langle n\rangle=0.65$ ).  $D_W$  is normalized to its maximum value at T=0.01; (b)  $\sigma(\omega)$  vs  $\omega$  parametric with  $\langle n\rangle$  at  $\lambda=1.5$ , T=1/10, and L=16 (results for L=10 are similar). The inset shows the lower  $J_H$ -split DOS at  $\langle n\rangle=0.93$ . In (a) and (b) a  $\delta$ -function broadening  $\epsilon=0.25$  was used, as well as set  $T_1$  for the hopping amplitudes.

A similar good agreement with experiments was observed working in the regime of the orbitally-induced PS but at a temperature above  $T_c^{PS}$ . Here the broad feature observed at high-T in Fig.4a moves to higher energies (Fig.4b) since  $\lambda$  has increased. At the temperature of the plot the system is an insulator at  $\langle n \rangle = 1$ , but as hole carriers are added a second peak at lower energies develop, in addition to a weak Drude peak (which carries, e.g., just 1% of the total weight at  $\langle n \rangle = 0.61$ ). This feature at high-T is reminiscent of recent experimental results [22] where a two-peak structure was observed at room-T and several densities. Similar results were obtained on  $4^2$  clusters. In Fig.4b the peak at large- $\omega$  is caused by phononic effects since its position was found to grow rapidly with  $\lambda$  ( $\Delta \sim 2\lambda \langle (Q^{(2)}_{\mathbf{i}}^2 + Q^{(3)}_{\mathbf{i}}^2)^{1/2} \rangle$ ). It corresponds to intersite transitions between Mn<sup>3+</sup> JTsplit states. The lower energy structure is compatible with a Mn<sup>3+</sup>-Mn<sup>4+</sup> transition [23]. The inset of Fig.4b

shows the DOS of the system. The two peaks above  $\mu$  are responsible for the features found in  $\sigma(\omega)$ . This interpretation is the same as given in Ref. [11] at  $D = \infty$ .

Summarizing, here the first computational study of the 2-orbital Kondo model including Jahn-Teller phonons was reported. The phase diagram includes regions of phase separation both at large and small  $e_q$ -density. One of them corresponds to a novel regime where PS is driven by the orbital, rather than spin, degrees of freedom. Coulomb interactions will break the large regions involved in PS for the pure  $H_{KJT}$  model into small islands of one phase embedded into the other. X-ray diffraction measurements should observe a coexistence of patterns characteristics of the two extreme stable phases, if the PS is static. If the process is more dynamical the Bragg peaks should be broad. Recalling that our spin-FM phase at  $\langle n \rangle = 1$  and D = 1, 2 is also compatible with Atype spin-AF order, several experimental results [7] are in agreement with the tendencies to PS discussed in this paper. In the limit of small  $\langle n \rangle$ , the PS observed here could be transformed by long-range Coulomb interactions into a charge-ordered state. Note that the PS observed in electron-doped Sr<sub>2</sub>MnO<sub>4</sub> [8] is also compatible with our results [24].

The authors are supported by the NSF grant DMR-9520776.

- S. Jin et al., Science 264, 413 (1994).
- [2] C. Zener, Phys. Rev. 82, 403 (1951).
- [3] S-W. Cheong and C. H. Chen, in *Colossal Magnetoresistance and Related Properties*, ed. by B. Raveau and C. N. R. Rao (World Scientific).
- [4] S. Yunoki et al., Phys. Rev. Lett. 80, 845 (1998); E. Dagotto et al., Phys. Rev. B 58, 6414 (1998).
- [5] S. Yunoki and A. Moreo, Phys. Rev. **B** 58, 6403 (1998).
- [6] See also E. L. Nagaev, Phys. Status Solidi (b) 186, 9 (1994); D. Arovas and F. Guinea, cond-mat/9711145; M. Yu. Kagan, et al., cond-mat/9804213.
- [7] J. W. Lynn et al., Phys. Rev. Lett. 76, 4046 (1996); J. M. De Teresa et al., Nature (London) 386, 256 (1997); G. Allodi et al., Phys. Rev. B 56, 6036 (1997); D. E. Cox et al., Phys. Rev. B 57, 3305 (1998); M. Hennion et al., Phys. Rev. Lett. 81, 1957 (1998); J. H. Jung et al., cond-mat/9809107; and references therein.
- [8] Wei Bao et al., Solid State Comm. 98, 55 (1996).
- A. J. Millis, et al., Phys. Rev. Lett. 74, 5144 (1995); H.
   Röder, et al., Phys. Rev. Lett. 76, 1356 (1996). A. J.
   Millis, et al., Phys. Rev. B 54, 5405 (1996).
- [10] Y. Murakami et al., Phys. Rev. Lett. 80, 1932 (1998).
- [11] Results using the  $D = \infty$  approximation can be found in A. J. Millis et al., Phys. Rev. **B 54**, 5405 (1996).
- [12] This approximation was shown to be accurate in Ref. [4].

- [13] Most of the work in one-dimension (1D) has been performed using  $t_{11} = t_{22} = 2t_{12} = 2t_{21}$  (set  $T_1$ ), but results have also been obtained with  $t_{11} = t_{22}$  and  $t_{12} = t_{21} = 0$  $(T_2)$ , as well as with the hopping that takes into account the proper orbital overlap, namely  $t_{11} = 3t_{22} = \sqrt{3}t_{12} =$  $\sqrt{3}t_{21}$  (T<sub>3</sub>) (see S. Ishihara et al., Phys. Rev. **B** 56, 686 (1997)). In two-dimensions (2D), the set  $T_1$  in both directions was used, but also the combination of  $T_3$  in the y-direction and  $t_{11} = 3t_{22} = -\sqrt{3}t_{12} = -\sqrt{3}t_{21}$   $(T_4)$ in the x-direction. Finally, in three-dimensions (3D)  $T_4$ was used in the x-direction,  $T_3$  in the y-direction, and  $t_{11}=t_{12}=t_{21}=0,\,t_{22}=4/3\,(T_5)$  in the z-direction. [14] Note that estimations of  $T_c^{FM}$  using quantum and clas-
- sical phonons lead to very similar results [9].
- [15] T. G. Perring et al., Phys. Rev. Lett. 78, 3197 (1997).
- [16]  $H_{KJT}$  is not invariant under arbitrary pseudospin-space rotations and, thus, the Mermin-Wagner theorem does not apply to the orbital correlations.
- [17] J. B. Goodenough, Phys. Rev. 100, 565 (1955); K. I. Kugel and D. I. Khomskii, JETP Lett. 15, 446 (1972); S. Ishihara et al., Phys. Rev. **B** 55, 8280 (1997); T. Mizokawa and A. Fujimori, Phys. Rev. **B** 56, R493 (1997).
- [18] Studies at larger values of  $\lambda$ 's are too costly in CPU time.
- [19] In Ref. [11], a MIT at  $\lambda \sim 1$  was also found but it was not associated with orbital order.
- [20] Slave-fermion studies of a model with strong Coulomb interactions and no phonons by S. Maekawa et al. (private communication) also found a similar PS.
- [21] M. Quijada et al., cond-mat/9803201. See also S. G. Kaplan et al., Phys. Rev. Lett. 77, 2081 (1996); Y. Okimoto et al., Phys. Rev. **B** 55, 4206 (1997); T. Ishikawa et al., Phys. Rev. **B** 57, R8079 (1998).
- [22] J. H. Jung et al., Phys. Rev. **B** 57, R11043 (1998); K. H. Kim et al., cond-mat/9804167 and 9804284.
- [23] Although its dependence with  $\lambda$  was weak.
- [24] Upon completion of this work we learned of experiments where the coexistence of orbitally-ordered and FMmetallic domains has been observed in Mn-perovskites (P. G. Radaelli et al., Second International Conference on Stripes and High Tc Superconductivity, Rome, June 2-6 (1998)). The present paper was presented at the same conference by one of the authors (A.M.).